Rare Metal Materials and Engineering
Volume 53, Issue 6, June 2024
Available online at www.rmme.ac.cn

Science Press

Cite this article as: Yang Yu, Chen Geng, Li Hui, et al. Preparation of Nanoscale (VNbTaZrHf)C High-Entropy Carbides via Molten Salt Electro-deoxidation and Its Catalytic Performance of Hydrogen Evolution Reaction[J]. Rare Metal Materials and Engineering, 2024, 53(06): 1566-1573. DOI: 10.12442/j.issn.1002-185X.20230580.

ARTICLE

Preparation of Nanoscale (VNbTaZrHf)C High-Entropy Carbides via Molten Salt Electro-deoxidation and Its Catalytic Performance of Hydrogen Evolution Reaction

Yang Yu[1], Chen Geng[2], Li Hui[2], Liang Jinglong[2], Hu Meilong[3], Hu Mengjun[4]

[1] Comprehensive Testing and Analyzing Center, North China University of Science and Technology, Tangshan 063009, China; [2] College of Metallurgy and Energy, North China University of Science and Technology, Tangshan 063210, China; [3] College of Materials Science and Engineering, Chongqing University, Chongqing 400044, China; [4] Key Laboratory of Material Processing and Mold Technology, School of Mechanical Engineering, Chongqing Industry Polytechnic College, Chongqing 401120, China

Abstract: The nanoscale (VNbTaZrHf)C high-entropy carbide (HEC) powders with face-centered cubic structure were prepared by electro-deoxidation of metal oxides and graphite in $CaCl_2$ at 1173 K. Appropriate temperature conditions are favorable for suppressing the in-situ sintering growth of HEC particles. Electrochemical performance tests were conducted in 1 mol/L KOH solution to investigate the catalytic performance of (VNbTaZrHf)C HEC. The catalytic performance of (VNbTaZrHf)C HEC for hydrogen evolution reaction (HER) was evaluated through polarization curves, Tafel slope, electrochemical impedance spectroscopy, and double-layer capacitance value cyclic voltammetry tests. Results show that the double-layer capacitance value of (VZrHfNbTa)C HEC is 40.6 mF/cm^2. The larger the double-layer capacitance value, the larger the electrochemically active surface area. Due to the high-entropy effect and nanoscale structure of (VNbTaZrHf)C HEC, it exhibits superior catalytic performance to HER. This research provides a novel method for the preparation of HECs via molten salt electro-deoxidation.

Key words: high-entropy carbide; molten salt electro-deoxidation; catalytic performance

Yeh[1] and Cantor[2] et al synthesized multi-component alloys with single-phase crystal structure and proposed the concept of entropy stabilization in 2004. As a result, the idea of entropy stabilization attracts much attention. Various factors, such as chemistry, crystallography, and the design of different component composition, offer endless possibilities for the development of new alloys with excellent mechanical, oxidation-resistant, thermal, and corrosion-resistant properties. The concept of entropy stabilization materials has recently expanded into high-entropy carbides (HECs), borides, nitrides, and oxides in high-entropy ceramics.

HECs gain widespread attention due to their exceptional mechanical, oxidation-resistant, and corrosion-resistant properties. Han et al[3] synthesized $VNbMoTaWC_5$ and $TiVNbTaWC_5$ HECs by low-pressure carbothermal shock method and prepared SiC with excellent thermal stability and antioxidant capacity. Li et al[4] achieved uniform composition and low oxygen content in single-phase (ZrTiTaNbMo)C powders by magnesium thermal reduction at 1623 K. Kovalev et al[5] prepared equimolar (TiZrHfNbTa)C HEC powders through high-energy ball milling, and the HEC powders exhibited excellent thermal stability. Xia et al[6] prepared (NbMoTaW)C and (NbMoTaWHf)C HECs with good mechanical properties using NbC, MoC, TaC, WC, and HfC powders as raw materials through the arc melting method. Although various methods, such as carbothermal reduction, magnesiothermic reduction, high-energy ball milling, and arc melting, have been used to synthesize HECs, the obtained materials are generally at the micrometer level and cannot be effectively applied in the electrocatalytic hydrogen evolution reaction (HER).

In electrochemical hydrolysis, the reaction at the cathode is

Received date: September 14, 2023
Foundation item: Chongqing Natural Science Foundation (cstc2021jcyj-msxmX1049); Tangshan Science and Technology Innovation Team Training Plan Project (21130207D)
Corresponding author: Hu Mengjun, Ph. D., Key Laboratory of Material Processing and Mold Technology, School of Mechanical Engineering, Chongqing Industry Polytechnic College, Chongqing 401120, P. R. China, E-mail: humj@cqipc.edu.cn

Copyright © 2024, Northwest Institute for Nonferrous Metal Research. Published by Science Press. All rights reserved.

considered as HER. HER is a promising green approach to produce hydrogen from renewable energy sources, and its efficiency depends on the electrocatalyst[7–15]. Noble metals, such as Pt[16–18], Ir[19–21], and Pd[22–23], possess excellent electrocatalytic performance, but the high cost restricts their industrial production. Transitional metal phosphides[24–26], sulfides[27–29], carbides[30–32], and nitrides[33–35] have emerged as new materials for HER electrocatalysts due to their low preparation cost, diverse types, and environmentally friendly characteristic. However, the catalytic activity and stability of these materials are inferior. The high-entropy material exhibits better electrocatalytic water decomposition performance due to the continuous distribution of self-adsorption, easy control of electronic structure, and excellent structural stability. High-entropy alloys (HEAs), nitrides, sulfides, and phosphides are considered as the new generation electrocatalysts, relying on four core effects[36-37]. The ZrHfNbTa series ceramic HEA is the new research direction of HEAs. Adding V element to the system can effectively improve the mechanical properties of materials, and five metal ions can be combined with carbon to form covalent and ionic bonding in (VZrHfNbTa)C HEC materials. These materials have high adjustability in component and structure, showing great potential in the electrocatalysis field. However, the investigation of HECs as electrocatalyst is still at the infancy stage because the synthesis of nano-scale HEC materials is still challenging and costly.

In this research, VNbTaZrHf HEA and (VZrHfNbTa)C HEC powders were prepared through the one-step preparation method, which involved the direct electro-deoxidation of the stoichiometric metal oxides and graphite in the molten $CaCl_2$ at 1173 K. A three-terminal electrochemical cell was used to investigate the catalytic performance of these HEC powders for hydrogen precipitation.

1 Experiment

The raw materials used in this research were mixed powders of Ta_2O_5, ZrO_2, Nb_2O_5, HfO_2, VO_2, and graphite. VNbTaZrHf HEA and (VNbTaZrHf)C HEC were separately prepared according to the molar ratio of oxides and graphite with the total mass of 2 g. A binder was prepared by dissolving 0.04 g polyethylene glycol in isopropanol, then it was added to the raw material, and finally the mixed material was uniformly ground. The mixed material was dried at room temperature and pressed into samples at the pressure of 10 MPa using cylindrical grinding tool with diameter of 25 mm. Finally, the pressed samples were sintered at 523 K for 3 h.

The water-free $CaCl_2$ (500 g) was placed in a corundum crucible and vacuum-dried at 673 K for 12 h. Then, the crucible was heated to 1173 K in a reactor with nickel flakes and graphite rods as the cathode and anode, respectively. The molten salt was pre-electrolyzed at 2.8 V to remove impurities and water. The cathode was made of mixed oxide precursors, and the anode was made of a graphite rod with diameter of 1 cm and height of 10 cm. The molten salt was subjected to electro-deoxidation at 3.1 V for 10 h. Finally, the products were cleaned by ultrasound, dried, and fully ground at 373 K.

The electrolytic voltage was provided by direct current power supply (DP310, MESTEK, Shenzhen, China). The phase of precursors and electro-deoxidation products was examined by X-ray diffractometer (XRD, D/max 2500PC, Rigaku, Japan). The microstructure and element distribution of precursors and electro-deoxidation products were characterized by scanning electron microscope (SEM, TESCAN VEGA II with Oxford INCA Energy 350) at backscattered electron (BSE) mode, energy dispersive spectrometer (EDS), field emission SEM (FESEM, ThermoFisher Scientific Quattro S), scanning transmission electron microscope (STEM, ThermoFisher Scientific Talos F200S), and high resolution transmission electron microscope (HRTEM). X-ray photoelectron spectroscope (XPS, ThermoFisher Scientific ESCALAB250Xi) was used to determine the elements of products and their oxidation states.

The electrochemical performance of HEC and HEA was evaluated by Chenhua CHI 660 instrument (Shanghai Chenhua Instrument Co. Ltd., China). The working electrodes were made by 80wt% VNbTaZrHf or (VNbTaZrHf)C powder+ 10wt% binder (polyvinylidene fluoride) +10wt% conductive agent (carbon black) +solvent (N-methyl pyrrolidone). The reference electrode was Ag/AgCl, and the counter electrode was platinum sheet.

The electrolyte was 1 mol/L KOH solution, and the area of electrode sheet immersed in the test solution was 1 cm^2. The conversion equation from Ag/AgCl reference electrode to reversible hydrogen electrode (RHE) is shown in Eq. (1), as follows:

$$E(\mathrm{RHE})=E(\mathrm{Ag/AgCl})+0.0591\times \mathrm{pH\ value}+0.197 \quad (1)$$

where E is the potential.

According to Eq. (1), the measured potential difference was 0.2224 V. The potentials measured in subsequent tests were converted to the ones concerning RHE. The catalytic properties of the prepared materials were studied through linear sweep voltammetry (LSV), cyclic voltammetry (CV) method, AC impedance spectroscopy (EIS) method, and Tafel curves.

2 Results and Discussion

2.1 Electro-deoxidation of mixed raw material powders

Fig. 1 displays XRD patterns of the VNbTaZrHf HEA and (VNbTaZrHf)C HEC precursors. Notably, the characteristic diffraction peaks of the oxides can be observed and no new phase can be detected. This result unequivocally demonstrates that the oxide mixture precursor remains inert to the chemical reactions, even after sintering treatment at 573 K for 3 h. During the sintering process, the oxide mixture precursor combines with binder to form a cohesive substance.

Fig. 2 shows SEM-BSE images and EDS element distributions of VNbTaZrHf HEA and (VNbTaZrHf)C HEC precursors. As shown in Fig. 2a, the constituents of VNbTaZrHf HEA precursor exhibit a homogeneous dispersion: no apparent agglomeration or sintering traces can

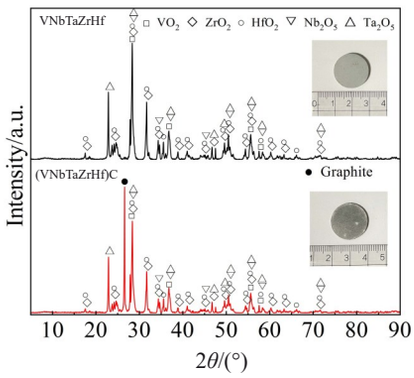

Fig.1 XRD patterns of VNbTaZrHf HEA and (VNbTaZrHf)C HEC precursors

be observed between the particles. Distinct powder particles are discernible, and the sintering marks can hardly be observed. The graphite phase is represented by the black particles, as shown in Fig. 2b. This further confirms that no chemical reaction occurs in the precursor during sintering at 573 K for 3 h. Furthermore, EDS analysis reveals the variation in the uniformity of particle sizes among different oxide phases. Specifically, Nb_2O_5, VO_2, and ZrO_2 exhibit relatively larger particle sizes, resulting in their aggregation, and the distribution of other phases is more uniform.

2.2 Structure and morphology characterization

Fig. 3 shows XRD patterns of the reduced products of VNbTaZrHf HEA and (VNbTaZrHf)C HEC samples after electro-deoxidation process. It can be observed that the products consist of body-centered cubic (bcc) HEAs and face-centered cubic (fcc) HECs. The electrolysis process obeys the deoxidation mechanism to form elemental metals and then promote the alloying process. Additionally, it is commonly reported that the electro-deoxidation process of HECs involves the release of metals from their oxides and an in-situ reaction with surrounding graphite atoms[38].

Fig. 4 shows SEM-BSE images and EDS element distributions of VNbTaZrHf HEA and (VNbTaZrHf)C HEC

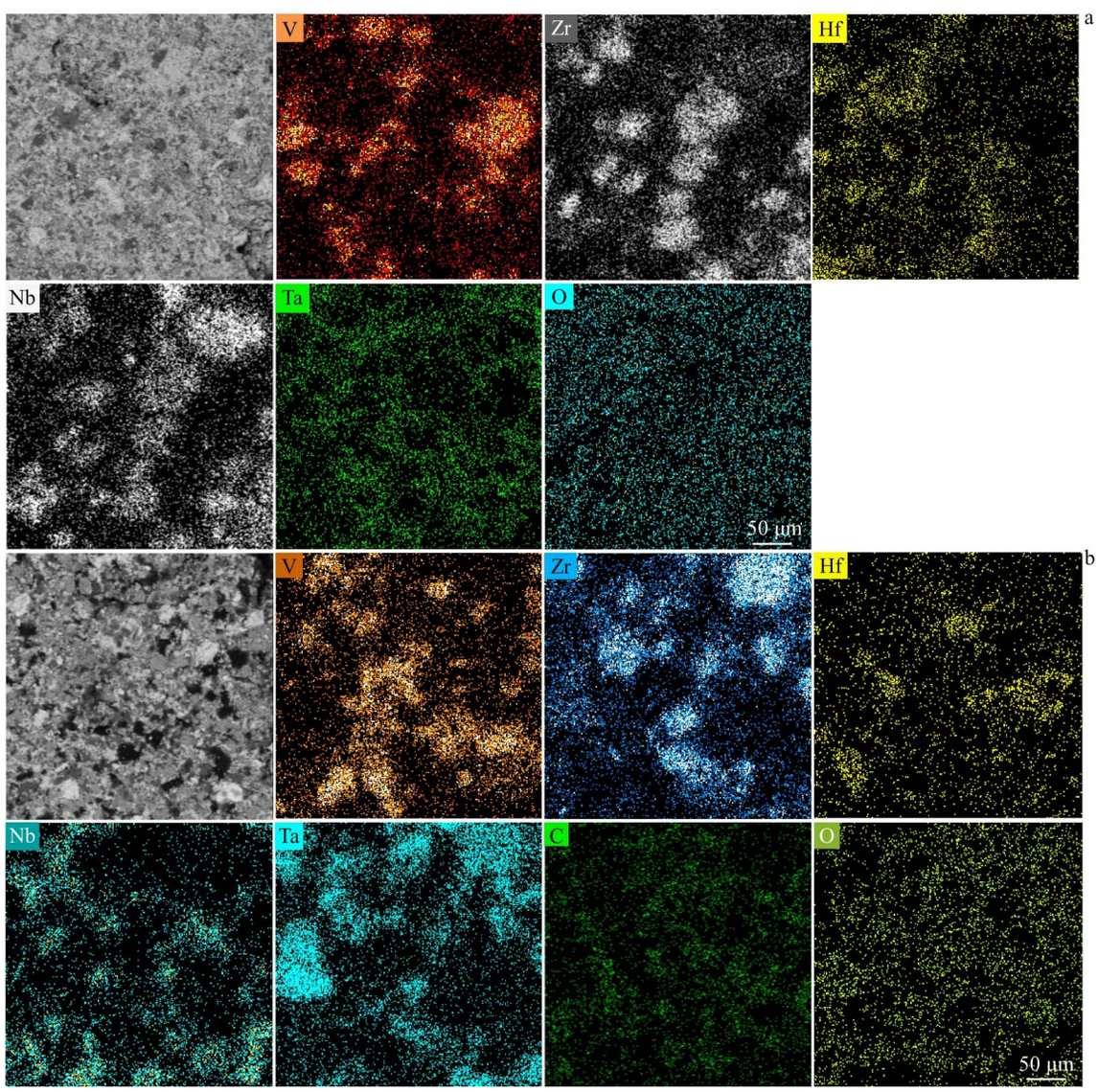

Fig.2 SEM-BSE images and EDS element distributions of VNbTaZrHf HEA (a) and (VNbTaZrHf)C HEC (b) precursors

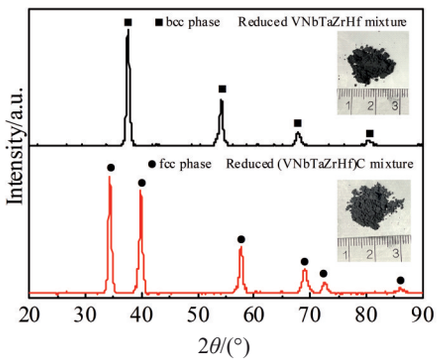

Fig.3 XRD patterns of reduced products of VNbTaZrHf HEA and (VNbTaZrHf) HEC samples

after electro-deoxidation process. As shown in Fig. 4a, the powder particles are nodular and the nodular particle size is approximately 1 μm. As shown in Fig.4b, the reduced product has aggregates with sizes smaller than 500 nm. It can be seen that the particle size of HECs is significantly smaller than that of HEAs due to the inhibition of particle growth during the moderate temperature electro-deoxidation process. The deoxidation temperature has no significant effect on the in-situ sintering of the (VNbTaZrHf)C HEC particles with high melting point, resulting in the smaller particle sizes. EDS analysis reveals that the elements are uniformly distributed within the particles. According to the quantitative analysis data in Table 1, the atomic ratio of the two products is close to the designed atomic ratio of the alloy.

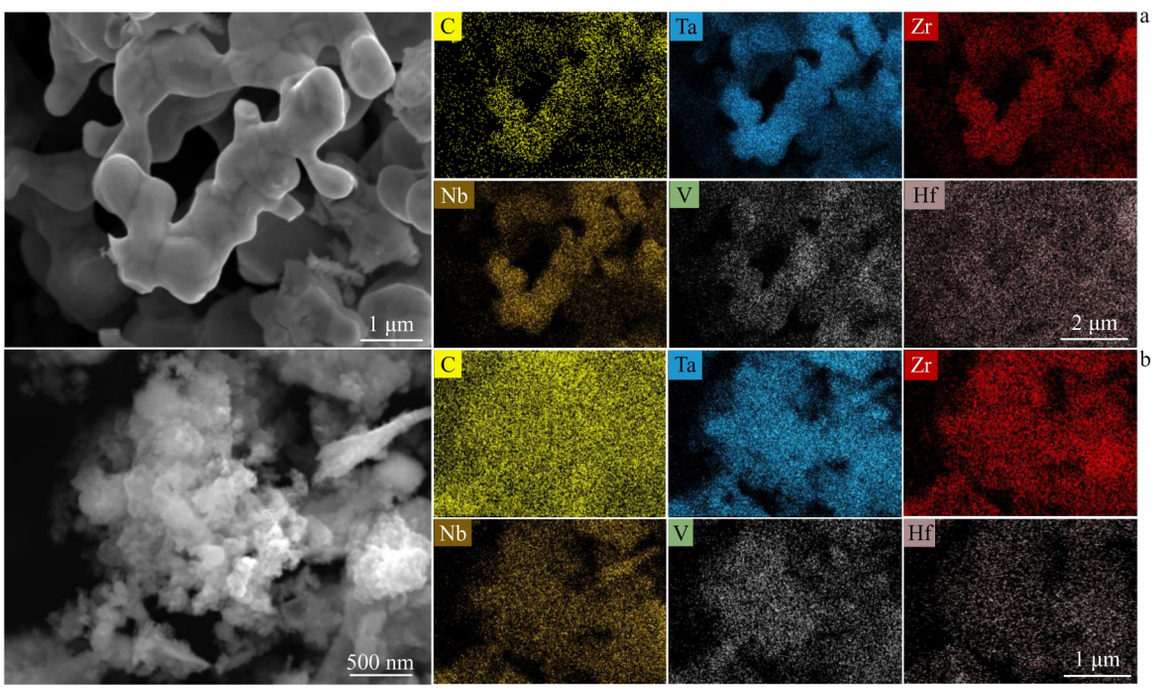

Fig.4 SEM-BSE images and EDS element distributions of VNbTaZrHf HEA (a) and (VNbTaZrHf)C HEC (b) after electro-deoxidation process

Table 1 EDS quantitative analysis results of VNbTaZrHf HEA and (VNbTaZrHf)C HEC after electro-deoxidation process (at%)

Powder	C	V	Zr	Hf	Nb	Ta	O
VNbTaZrHf HEA	0.94	18.67	21.47	21.06	19.35	17.44	1.07
(VNbTaZrHf)C HEC	61.1	5.27	9.31	9.26	7.34	6.66	1.11

Fig. 5 shows STEM images, EDS surface scanning results, HRTEM images, and corresponding fast-Fourier transform (FFT) patterns of the VNbTaZrHf HEA and (VNbTaZrHf)C HEC after electro-deoxidation process. According to STEM images, the VNbTaZrHf HEA powder has a dense block-like structure, and the (VNbTaZrHf)C particles have smaller sizes of less than 100 nm and exhibit cluster-like morphology. The STEM-EDS results demonstrate the uniform distribution of elements. HRTEM images reveal the polycrystalline nature of the product particles of VNbTaZrHf HEA and (VNbTaZrHf)C HEC. FFT patterns display discontinuous diffraction rings, indicating that VNbTaZrHf HEA has bcc structure, whereas (VNbTaZrHf)C HEC has fcc structure.

Fig. 6 shows XPS full-spectra analysis of the product powders of VNbTaZrHf HEA and (VNbTaZrHf)C HEC samples. The result indicates that both product powders contain the corresponding elements and a small amount of residual oxygen from the alloy. The VNbTaZrHf HEA powder has a small amount of cathodic carbon deposition, suggesting that the electro-deoxidation products are not contaminated by the impurities from the molten salt. High-resolution XPS results demonstrate the existence of strong interactions among the elements in both products. However, a small amount of Zr in the VNbTaZrHf HEA can be observed in the form of oxides, and Nb is susceptible to oxidation, thereby forming NbO after air exposure.

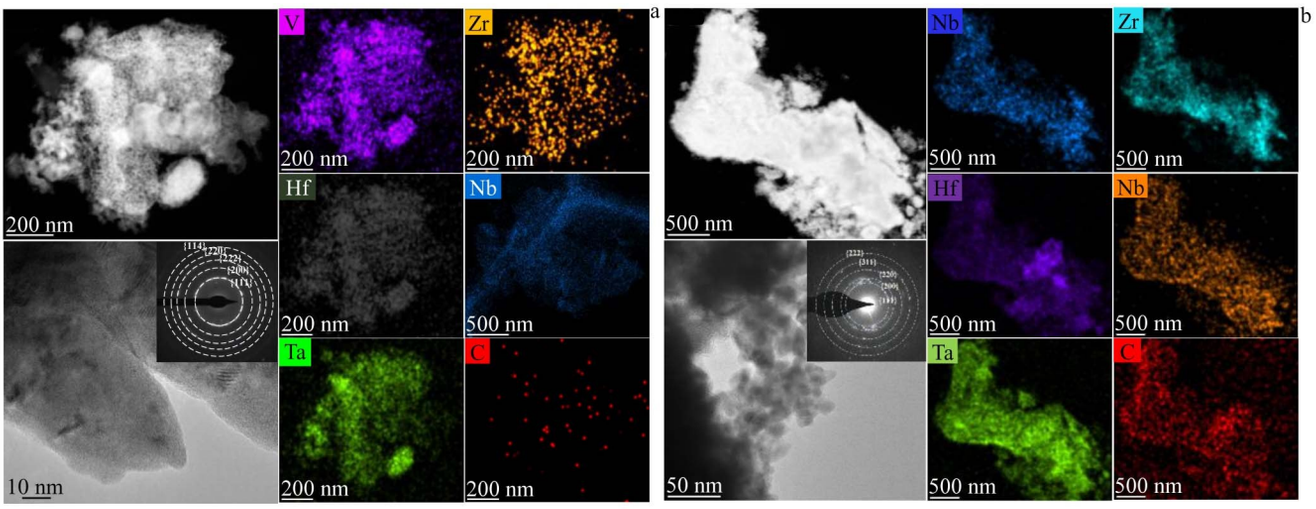

Fig.5 STEM images, EDS surface scanning results, HRTEM images, and corresponding FFT patterns of VNbTaZrHf HEA (a) and (VNbTaZrHf)C HEC (b) after electro-deoxidation process

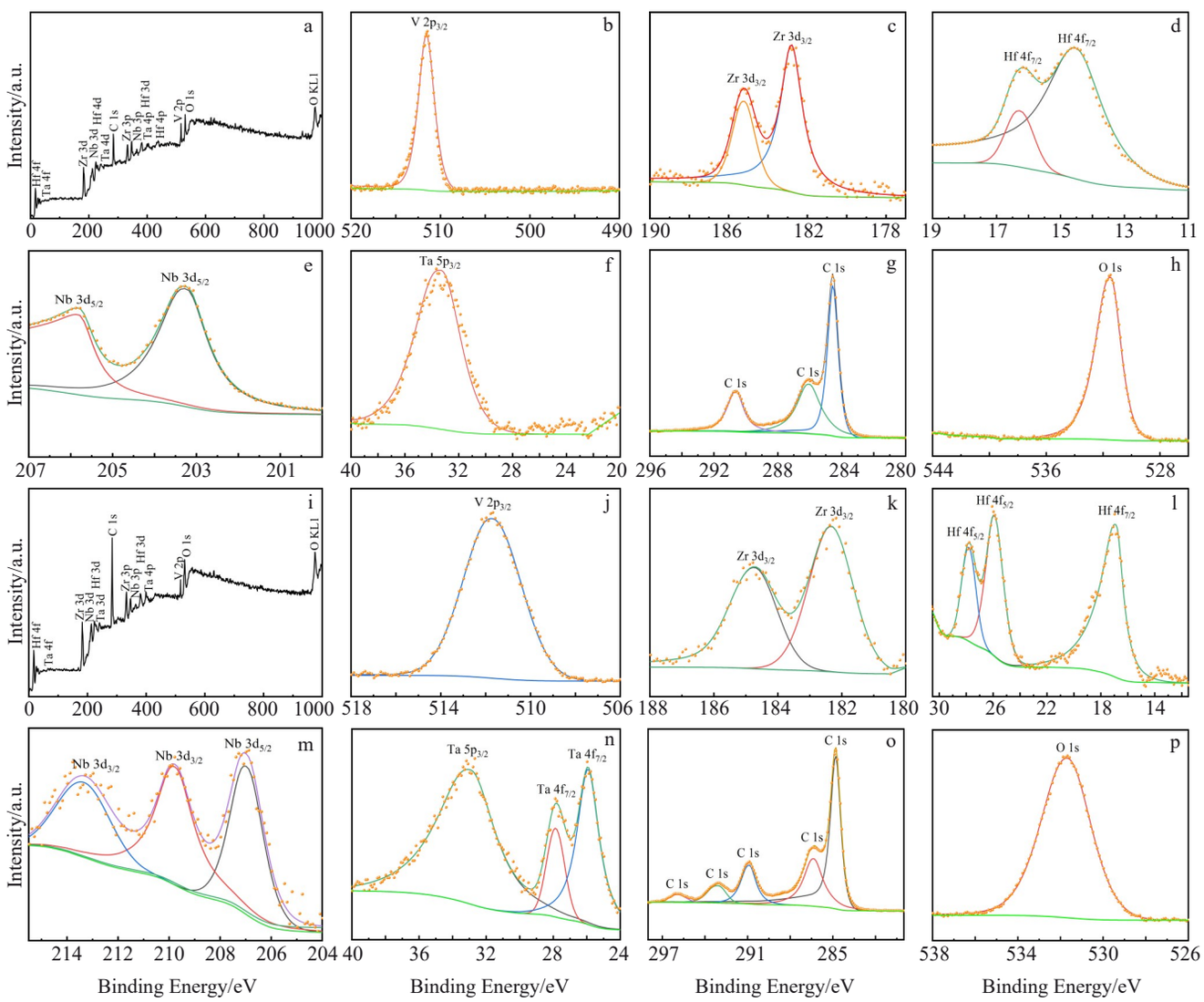

Fig.6 XPS spectra and high-resolution XPS spectra of VNbTaZrHf HEA (a–h) and (VNbTaZrHf)C HEC (i–p) after electro-deoxidation process: (a, i) overall spectra; (b, j) V element; (c, k) Zr element; (d, l) Hf element; (e, m) Nb element; (f, n) Ta element; (g, o) C element; (h, p) O element

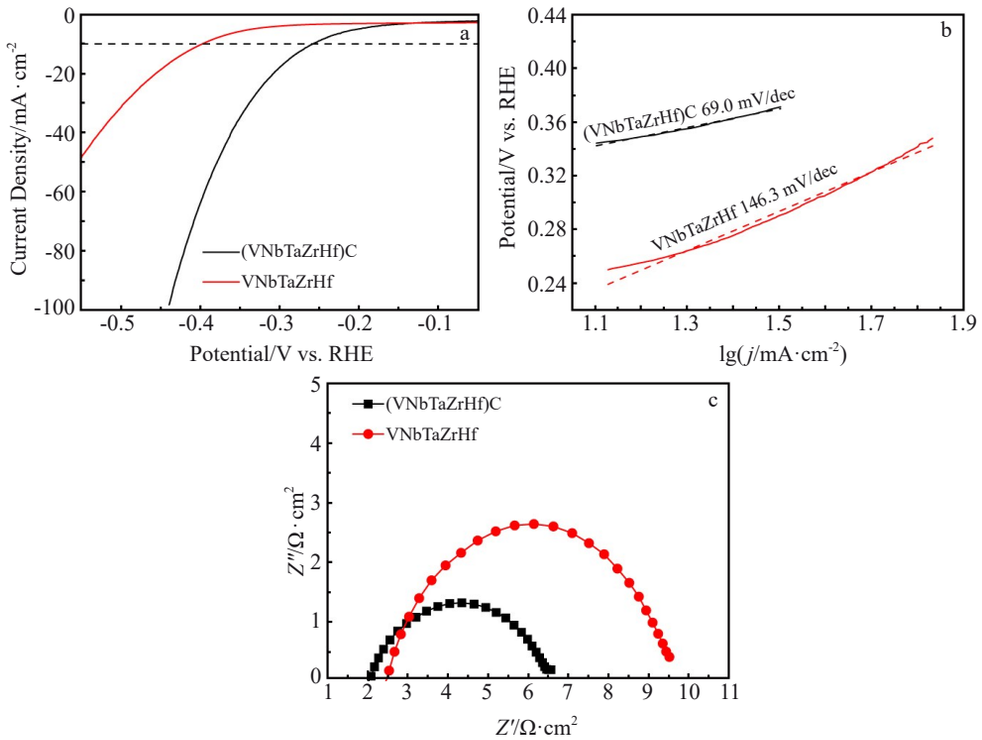

Fig.7 Polarization curves (a), Tafel plots (b), and EIS results (c) of (VNbTaZrHf)C HEC and VNbTaZrHf HEA samples

2.3 Catalytic hydrogen precipitation performance of (VNbTaZrHf)C HEC powder

The electrochemical HER performance of the VNbTaZrHf HEA and (VNbTaZrHf)C HEC catalysts was tested in 1 mol/L KOH electrolyte. Fig. 7a displays HER polarization curves of VNbTaZrHf HEA and (VNbTaZrHf)C HEC samples. It can be observed that (VNbTaZrHf)C HEC has an overpotential of 258.8 mV at the current density of 10 mA/cm^2, which is much lower than that of VNbTaZrHf HEA (398.2 mV). This result indicates that the catalytic activity of (VNbTaZrHf)C HEC is higher than that of VNbTaZrHf HEA, which is possibly due to the strong electronic interactions resulting from the addition of carbon element. Fig. 7b shows the fitted Tafel plots of VNbTaZrHf HEA and (VNbZrHf)C HEC samples, presenting the reaction kinetics in the electrochemical process. The Tafel slope results in Fig.7b and Table 2 show that the Tafel slope of (VNbTaZrHf)C HEC (69.0 mV·dec^{-1}) is much smaller than that of Pt/C (99 mV·dec^{-1}) and Ir/C (122 mV·dec^{-1}). It is also much smaller than the Tafel slope of VNbTaZrHf HEA (146.3 mV·dec^{-1}). Smaller Tafel slope indicates better reaction kinetics. There-fore, the reaction kinetics of (VNbTaZrHf)C HEC is much better than that of VNbTaZrHf HEA. Fig. 7c shows EIS results of (VNbTaZrHf)C HEC and VNbZrHfTa HEA samples. The obtained EIS curve has a typical semicircular arc shape. Generally, the smaller the radius of arc curvature, the lower the resistance against the charge transport. Through comparison, it is found that the radius of curvature of VNbTaZrHf HEA is larger, which means that the charge transfer resistance is higher. Increasing the electrical conductivity of the products can reduce the resistance against charge transport, and the carbon content in the product is closely related to the electrical conductivity. The addition of carbon is beneficial to improve the conductivity of the products, therefore reducing the resistance against charge transfer and ultimately improving the kinetics of catalytic reactions.

Table 2 Comparison of Tafel slopes of (VNbTaZrHf)C HEC, VNbTaZrHf HEA, and commonly used HER electro-catalysts

Electro-catalyst	Pt	Ir	HEC	HEA
Tafel slope/mV·dec^{-1}	99	122	69.0	146.3

Fig. 8a – 8b display CV test results of VNbTaZrHf HEA and (VNbTaZrHf)C HEC samples to determine their double-layer capacitance values. Fig. 8c shows the fitted capacitance curve with the current density as the vertical coordinate and the corresponding scanning rate as the horizontal coordinate. The slope of the fitted line in Fig. 8c can reflect the magnitude of the double-layer capacitance value of corresponding material. Since the double-layer capacitance value of material is proportional to the electrochemically active area, the electrochemically active area is used to compare the double-layer capacitance values in this research. The double-layer capacitance of (VNbTaZrHf)C HEC is 40.6 mF/cm^2, which is larger than that of VNbTaZrHf HEA (26.8 mF/cm^2). This result indicates that the addition of C element increases the number of active sites and has a significant effect on the activity of active sites.

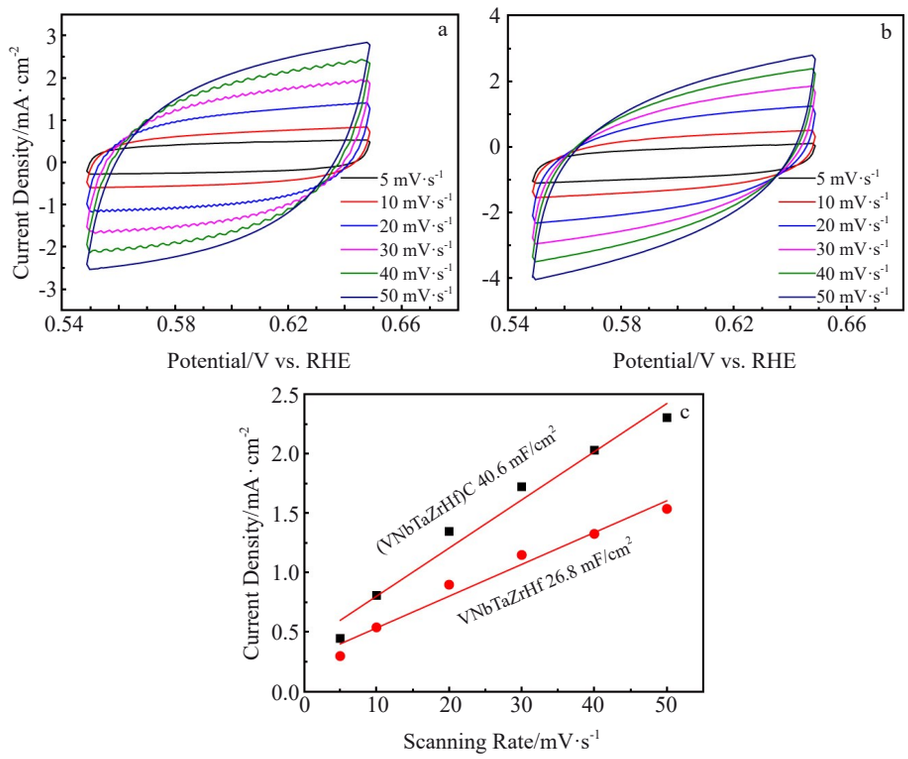

Fig.8 CV curves of VNbTaZrHf HEA (a) and (VNbTaZrHf)C HEC (b); calculated double-layer capacitance of VNbTaZrHf HEA and (VNbTaZrHf)C HEC (c)

3 Conclusions

1) The overpotential of (VNbTaZrHf)C HEC and VNbTaZrHf HEA is 258.8 and 398.2 mV at the current density of 10 mA/cm^2, respectively. The Tafel slope of (VNbTaZrHf)C HEC and VNbTaZrHf HEA is 69 and 146.3 mV/dec, respectively. EIS curves of both (VNbTaZrHf)C HEC and VNbTaZrHf HEA have typical semi-circular shapes, and the curvature radius of (VNbTaZrHf)C HEC is smaller.

2) The addition of carbon enhances the electrical conductivity of HEC and reduces the charge transfer resistance, improving the catalytic reaction kinetics.

3) The double-layer capacitance value of (VNbTaZrHf)C HEC is 40.6 mF/cm^2, whereas that of VNbTaZrHf HEA is 26.8 mF/cm^2, indicating that the catalytic performance of nanoscale (VNbTaZrHf)C HEC powders is significantly better than that of VNbTaZrHf HEA. This research provides new idea for the preparation of HECs via molten salt electrodeoxidation and expands the types of catalytic materials.

References

1 Yeh J W, Chen S K, Lin S J *et al*. *Advanced Engineering Materials* [J], 2004, 6(5): 299

2 Cantor B, Chang I T H, Knight P *et al*. *Materials Science and Engineering A*[J], 2004, 375–377: 213

3 Han Y C, Liu M L, Sun L *et al*. *Proceedings of the National Academy of Sciences*[J], 2022, 119(37): e2121848119

4 Li B Q, Liu C, Fang Z *et al*. *Journal of the European Ceramic Society*[J], 2022, 42(15): 6767

5 Kovalev D Y, Kochetov N A, Chuev I I. *Ceramics International*[J], 2021, 47(23): 32626

6 Xia M, Lu N, Chen Y *et al*. *International Journal of Refractory Metals and Hard Materials*[J], 2022, 107: 105859

7 Wang W S, Liu H, Yu Z J *et al*. *Rare Metal Materials and Engineering*[J], 2023, 52(2): 461

8 Zhang Xiaoyan, Du Qiang, Yan Jinhua *et al*. *Rare Metal Materials and Engineering*[J], 2022, 51(3): 977 (in Chinese)

9 Sun Wei, Yang Jincheng, Mao Wanjun *et al*. *Rare Metal Materials and Engineering*[J], 2023, 52(5): 1963 (in Chinese)

10 Li Z J, Yang J H, Cheng C *et al*. *Rare Metal Materials and Engineering*[J], 2023, 52(10): 3608

11 Li Yaning, Li Guangzhong, Yang Baojun. *Rare Metal Materials and Engineering*[J], 2023, 52(3): 1022 (in Chinese)

12 Zhang Lei, Huang Juntong, Hu Zhihui *et al*. *Rare Metal Materials and Engineering*[J], 2022, 51(4): 1341 (in Chinese)

13 Shen Zhongwei, Zhang Jianli, Tang Yiping *et al*. *Rare Metal Materials and Engineering*[J], 2023, 52(4): 1303 (in Chinese)

14 Li Hongpeng, Jiang Yunbo, He Jianyun. *Rare Metal Materials and Engineering*[J], 2023, 52(4): 1345 (in Chinese)

15 Li Xide, Liu Yuzuo, Zhang Chuo *et al*. *Rare Metal Materials and Engineering*[J], 2022, 51(11): 4117 (in Chinese)

16 Yu P, Zheng R H, Ma H Z *et al*. *Journal of the Electrochemical Society*[J], 2022, 169(4): 044514

17 Dong B X, Tian H, Wu Y C *et al*. *International Journal of Hydrogen Energy*[J], 2016, 41(33): 14507

18 Liu W Q, Tang Y, Liu F *et al*. *International Journal of Hydrogen Energy*[J], 2023, 48(4): 1255
19 She L N, Zhao G Q, Ma T Y *et al*. *Advanced Functional Materials*[J], 2022, 32(5): 2108465
20 Yu Z P, Li Y F, Torres-Pinto A *et al*. *Applied Catalysis B: Environmental*[J], 2022, 310: 121318
21 Jiang M, Zhu D D, Zhao X B. *Journal of Energy Chemistry*[J], 2014, 23(1): 1
22 Yu P, Jiang H, Peng R *et al*. *Journal of Power Sources*[J], 2021, 483: 229175
23 Yu P, Ma J, Zhang R *et al*. *ACS Applied Energy Materials*[J], 2018, 1(2): 267
24 Barati D G, Maleki M, Toghraei A *et al*. *International Journal of Hydrogen Energy*[J], 2023, 48(11): 4253
25 Du M X, Li D, Liu S Z *et al*. *Chinese Chemical Letters*[J], 2023, 34(9): 108156
26 Nguyen T X, Ting N H, Ting J M. *Journal of Power Sources*[J], 2022, 552: 232249
27 Wen X, Yang X, Li S *et al*. *New Journal of Chemistry*[J], 2022, 46(8): 3555
28 Yang M, Jiang Y M, Liu S *et al*. *Nanoscale*[J], 2019, 11(29): 14016
29 Nouseen S, Singh P, Lavate S *et al*. *Catalysis Today*[J], 2022, 397–399: 618
30 Kuang M, Huang W, Hegde C *et al*. *Materials Horizons*[J], 2020, 7(1): 32
31 Zhu J P, Wu H B, Gui K G *et al*. *Chemical Communications*[J], 2022, 58(89): 12503
32 Tian Z, Wang Z, Yao P *et al*. *International Journal of Hydrogen Energy*[J], 2021, 46(80): 40203
33 Jiang K, Li K, Liu Y Q *et al*. *Electrochimica Acta*[J], 2022, 403: 139700
34 Badreldin A, Nabeeh A, Ghouri Z K *et al*. *ACS Applied Materials & Interfaces*[J], 2021, 13(45): 53702
35 Wang B, Lu M, Chen D *et al*. *Journal of Materials Chemistry A*[J], 2021, 9(23): 13562
36 Yong Z, Zuo T T, Tang Z *et al*. *Progress in Materials Science*[J], 2014, 61: 1
37 Xue Lian, Sun Hao, Cheng Wei *et al*. *Materials China*[J], 2023, 42(3): 249 (in Chinese)
38 Yang Y, Chen B, Chen J *et al*. *Canadian Metallurgical Quarterly*[J], 2022, 61(4): 389

熔盐电脱氧工艺制备纳米级(VNbTaZrHf)C高熵碳化物及其析氢反应的催化性能

杨　宇[1]，陈　庚[2]，李　慧[2]，梁精龙[2]，扈玫珑[3]，胡蒙均[4]
(1. 华北理工大学 综合测试分析中心，河北 唐山 063009)
(2. 华北理工大学 冶金与能源学院，河北 唐山 063210)
(3. 重庆大学 材料科学与工程学院，重庆 400044)
(4. 重庆工业职业技术学院 机械工程学院 材料成型及模具技术重点实验室，重庆 401120)

摘　要：通过在1173 K的$CaCl_2$中对金属氧化物和石墨进行电脱氧，制备了具有面心立方结构的纳米级(VNbTaZrHf)C高熵碳化物（HEC）粉末。适当的温度条件有利于抑制HEC颗粒的原位烧结生长。在1 mol/L KOH溶液中进行了电化学性能测试，探索(VNbTaZrHf)C HEC的催化性能。通过极化曲线、Tafel斜率、电化学阻抗谱和双层电容值CV测试评估了(VNbTaZrHf)C HEC的催化析氢反应（HER）性能。结果表明，(VNbTaZrHf)C HEC的双层电容值为40.6 mF/cm^2。双层电容值越大，表明电化学活性表面积越大。由于(VNbTaZrHf)C HEC的高熵效应和纳米级结构，它表现出优异的催化HER性能，并为通过熔盐电脱氧制备HECs提供了新方法。

关键词：高熵碳化物；熔盐电脱氧；催化性能

作者简介：杨　宇，男，1992年生，博士，讲师，华北理工大学综合测试分析中心，河北 唐山 063009，电话：0315-8816212，E-mail：yyu@ncst.edu.cn